Edge Flame Structure in a Non-Premixed Methane-Air Jet Flame

R. B. McCoy[1], H. N. Najm, J. Ray
Sandia National Laboratories
Livermore, CA, USA
&
J. E. Rehm, and P. H. Paul
Eksigent Technologies LLC
Livermore, CA, USA

Abstract

We present results from a numerical study of an edge flame at the base of a laminar 2D non-premixed methane jet flame in coflow air, with the GRI1.2 chemical mechanism. We focus the analysis on the detailed chemical structure and topology of the edge flame that forms in the mixing layer after the ignition. The initial triple-flame structure evolves with time, and relaxes to an edge flame composed of a lean premixed flame and a diffusion flame. The rich premixed branch shrinks and nearly disappears because of the steep equivalence ratio gradient in front of the flame on the rich side. Results show that reversing the sign of the jet shear layer (coflow greater than the jet velocity) has a small effect on the flame structure. The internal structure of the edge-flame reaction zones are presented. Comparison with experiments show good agreement in [OH], [CO] and the OH + CO = H + CO_2 forward reaction rate distributions. The distribution of the product [CH_2O][OH] bears strong spatial correlation to the distribution of [HCO] and the forward reaction rate of OH + CH_2O = HCO + H_2O and consequently the heat release rate.

Introduction

Edge flames can exist in many practical configurations where pockets of rich and lean mixtures coexist in close proximity and where partial premixing of fuel and oxidizer occurs. They are generally composed of three reaction zones (branches): a lean premixed branch, a rich premixed branch and a nonpremixed - diffusion flame branch; hence they are also known as triple or tribrachial flames. The two premixed branches form curved fronts behind which a diffusion flame develops and stabilizes.There has recently been a growing number of experimental, analytical and numerical studies of triple flames liftoff mechanism and flame stabilization [1, 2, 3], and on propagation speed of edge flames [4, 5, 6, 7]. Methane-air triple flames in particular were studied experimentally [8, 9] and numerically with a reduced chemical mechanism [10].

The aim of the present work is to conduct a detailed study of the internal chemical structure and topology of the edge flame at the base of a lifted non-premixed methane-air jet using a detailed C_1C_2 chemical mechanism. In order to analyze the effect of the strain-rate field on the edge flame structure, we investigate two jet shear layer conditions, one with the jet fuel stream faster than the coflow air stream, and another with the fuel stream slower than the coflow stream. We also present comparisons between numerical results and experimental measurements and analyze the possibility of utilization of simultaneous measurements of OH with CO, and CH_2O with OH, as well as measurements of HCO as observables for edge flame topology and heat release rate or reaction rate. The comparison between experimental measurements of CO and OH and the computed forward reaction rate CO+OH$\rightarrow$H+CO_2 is also presented.

[1]Corresponding author, email: rbmccoy@ca.sandia.gov

Formulation And Numerical Scheme

An Eulerian-Lagrangian low Mach number reacting 2D flow model was used in the simulations. The details of model formulation and numerical scheme can be found in [11, 12, 13, 14]. An Eulerian formulation of the energy and species conservation equations discretized on a multi-layered adaptive mesh is employed. The Lagrangian vortex method is adopted for the momentum equations, and an adaptive fast multipole method is used for the velocity evaluations. Since the domain of interest is open, the spatially uniform stagnation pressure is assumed to be constant in time. We also assume that the mixture has zero bulk viscosity and is a perfect gas. N_2 is regarded as dominant (as it is in fact in the mixture conditions investigated) such that the diffusion of any species in the mixture is approximated by binary diffusion into N_2 at the local temperature. Soret and Dufour effects and radiant heat transfer are neglected. The GRImech1.2 [15] C_1C_2 chemical mechanism is used, with 32 species and 177 reactions. A second-order upwind Godunov scheme is used for spatial discretization of convective terms. A coupled Lagrangian-Eulerian time integration approach is adopted based on a second-order Runge-Kutta predictor-corrector formulation for both the Lagrangian and Eulerian integrations. The overall solution proceeds with global Lagrangian time steps, within which are embedded Eulerian sub-steps. Operator splitting is used within the Eulerian sub-steps to allow efficient computations with detailed chemical source terms. An ODE integrator (CVODE) [16] was used to integrate the stiff chemical source terms.

Numercial Configuration Description

We compute the ignition and stabilization of a 2D laminar methane jet with coflow air. The methane stream is diluted 40% (by volume) with N_2, the domain size is 10 cm$\times$5 cm. The mesh cell sizes range from 1 mm to 15 μm, from the coarsest to the finest mesh respectively. The adaptive mesh grids and corresponding edge flame structure are shown in Fig.1. Boundary conditions include inflow at the bottom boundary, slip vertical walls, and an outflow top edge.

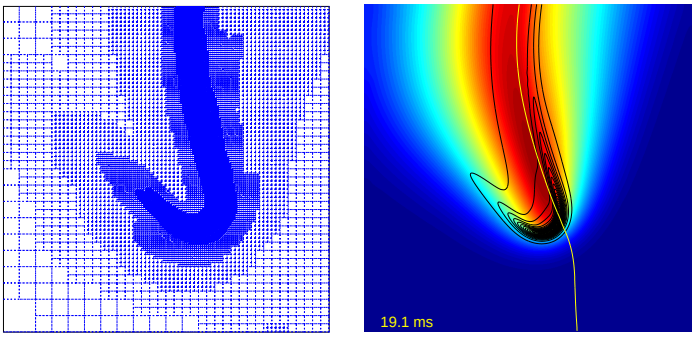

Figure 1: The adaptive meshes (left frame) and corresponding edge flame structure (right frame) are shown for the fully developed edge flame. In the right frame the structure and position of the flame is represented with the heat release contours in black and a yellow stoichiometric mixture fraction line. The color map presents mole fraction of CO_2, blue is mapped to the lowest value, red to the highest.

The flowfield is initialized with parallel streams of room-temperature air and CH_4 and then allowed to relax to a steady jet solution. The ignition is then initialized by transient heating of a small spot in the jet mixing layer 1 cm above the jet inlet for a duration of 1 ms. We study two configurations: case A with jet stream velocity of 0.8 m/s and coflow air velocity of 0.25 m/s and case B with fuel velocity of 0.25 m/s and coflow velocity of 0.8 m/s. The two studied cases are shown in Fig. 2, only left half of the domain is presented (5 cm $\times$ 5 cm). The left column shows

case A and the right column - case B. In the top plots row mole fraction of CH_4 is shown in color, the yellow line represents the stoichiometric mixture fraction line and the heat release rate for the flame fronts developed 4 ms after ignition started is shown as black contours. The upper plots in Fig. 2, represent the simulation at about 4ms after the ignition. The bottom row depicts the vertical velocity profile at the inlet. Studying these two configurations enables us to analyze the effect of the shear layer structure (faster fuel or oxidizer), and associated strain-rate fields, on the flame edge structure at the base of the lifted jet.

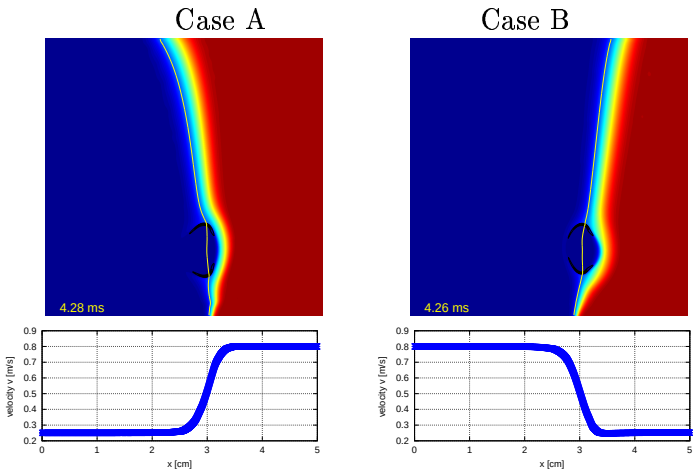

Figure 2: The two studied cases: case A is shown in the left column and case B in the right. The top row shows the mole fraction of CH_4 (color), the black contours represent heat release rate and the yellow line is the stoichiometric mixture fraction line. The bottom row shows the vertical velocity profiles at the inlet. The color map: blue is mapped to the lowest value, red to the highest.

An elemental mixture fraction is defined as in [17]

$$\xi^e = \frac{2Z_C/W_C + Z_H/(2W_H) + (Z_{O,2} - Z_O)/W_O}{2Z_{C,1}/W_C + Z_{H,1}/(2W_H) + Z_{O,2}/W_O},$$

where subscripts 1 and 2 refer to fuel and oxidizer streams respectively, and W_i is molar weight. Subscripts C, H, O refer to carbon, hydrogen and oxygen. Z_i is an elemental mass fraction, and denotes the ratio between the mass of an element i and the total mass,

$$Z_i = \sum_{j=1}^{S} \mu_{ij} w_j, \qquad i = 1, ..., M$$

where S is the number of species and M total number of elements in the mixture, coefficients μ_{ij} denote the mass proportion of the elements i in the species j and w_j is the mass fraction.

Ignition and Propagation of the Edge Flames

The ignition process is presented in Fig. 3, shown using the time evolution of the heat release rate. The yellow line represents the stoichiometric mixture fraction line. The top/bottom row corresponds to case A/B.

In case A, ignition was initiated in the lean premixed zone to the left of the stoichiometric mixture fraction line, while in case B ignition was started in the fuel rich region. In both cases the ignition front forms a circular front that grows and propagates through the stoichiometric line

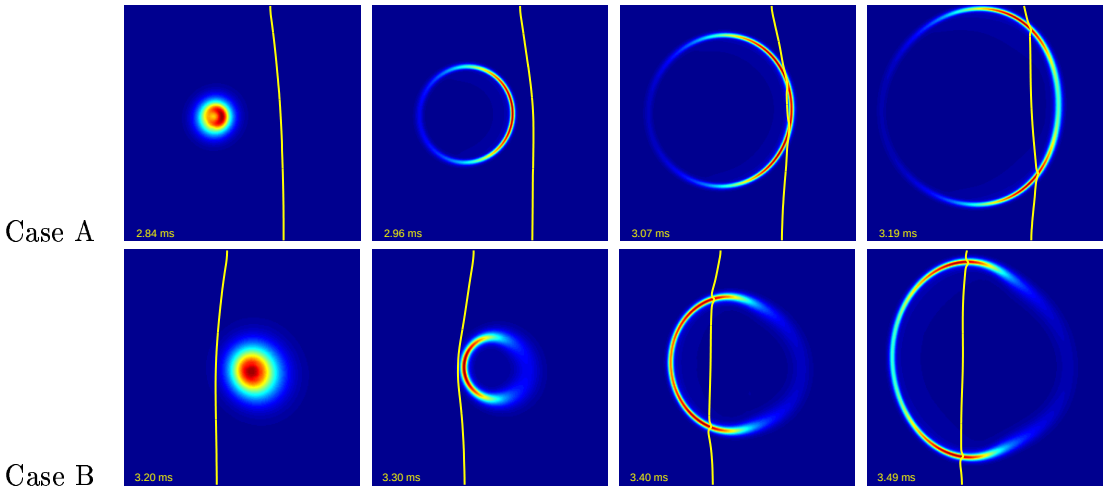

Figure 3: Ignition process presented as time evolution of heat release rate (color); the yellow line is the stoichiometric mixture fraction line. The top row corresponds to case A and the bottom to case B. The dimensions of the region shown are 6 mm×5 mm. Time is measured from the inception of heating for ignition.

eventually forming two edge flames that propagate up and down the stoichiometric mixture fraction line. The overall structure, topology and propagation of the ignition fronts, when viewed relative to the stoichiometric mixture fraction line, is similar for the two studied cases, and is independent on the ignition origin and the strain rate distribution.

The edge flames initially develop a triple-flame-like structure, at least as far as the global structure of the heat release rate field is concerned, as shown in Fig. 4 for three different time instances and for both cases. The edge flame structure consists of lean (on the left) and rich (on the right) premixed flame zones and the diffusion flame zone behind the premixed wings.

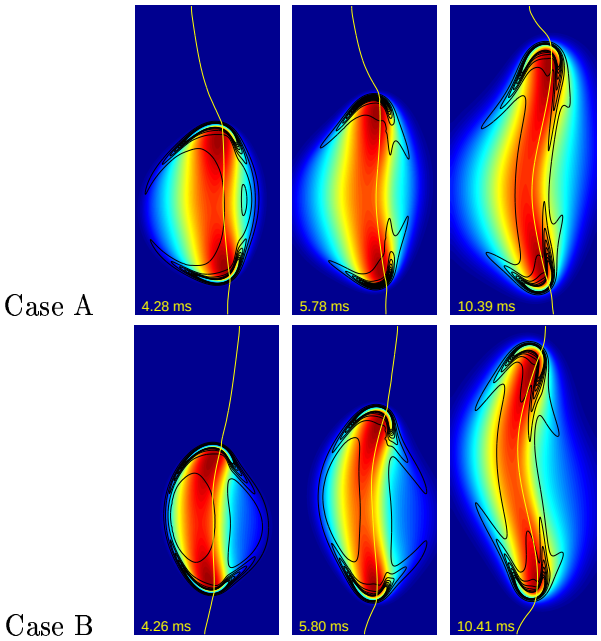

Figure 4: Evolution of the edge flames; contours represent heat release and the color field depicts mole fraction of CO_2. The top row corresponds to case A and the bottom to case B. Heat release contours near the maximum are not shown, so as to not obstruct the view. The yellow line is the stoichiometric mixture fraction line. The frame dimensions are 0.8 cm × 1.75 cm.

The maximum heat release rate is located in the lean premixed zone, in agreement with the observation in hydrogen-air triple flames [7]. One can also observe that the heat release rate initially outlines the lean and rich premixed wings (frames corresponding to ∼4.3 ms). However, at later time, the rich branch of heat release rate contours align along the fuel-side of the diffusion flame (frames corresponding to ∼10.4 ms). The edge flame's rich branch becomes very small, folds onto the trailing diffusion branch, and nearly disappears. This is due to a much equivalence ratio gradient (encountered immediately in front of the edge flame) on the rich side than on the lean side. Hence, on the rich side of the edge flame the flamability limit is more quickly met, and the rich premixed branch terminates.

The lower flame travels first downwards towards the jet inlet, but eventually is blown away and very slowly moves upwards with the velocity of 2.1 cm/s in case A and 3.5 cm/s in case B. The flame burning speed is 30.3 cm/s in case A and 31.5 cm/s in case B. The laminar premixed-flame burning speed S_L for the mixture used in the simulations is about 25.5 cm/s. Although no stable lift-off was achieved in either case for the flow conditions considered here, the structure of the edge flame has indeed stabilized. The transient changes in edge flame structure and internal peak quantities have subsided. Ongoing computations reveal that stable lift-off can be achieved for the jet velocity of 0.45 m/s and coflow velocity of 0.1 m/s, and confirm the achievement of stationary structure by the edge flames presented here.

The vertical velocity fields corresponding to cases A and B are shown in Fig. 5. The shear layer structure causes different tilting of the edge flames in the two cases and induces corresponding different stretching on the edge flame, but does not affect the internal flame chemical structure. The edge flames in both cases exist on the oxidizer side, thus not necessarily in the slow fluid region. The case with the faster oxidizer stream (B) exhibits faster downstream drift of the flame edge as indicated above. The mixing layer defines the structure, topology and position (relative to the stoichiometric mixture fraction line) of the edge flame. The tilting and stretching induced by the shear layer and associated strain rate fields can be seen in Fig. 5. Upward stretching of the rich side of the lower edge flame is seen in case A, whereas in case B the lean side of the lower edge flame is stretched, affecting the extent of the lean premixed branch.

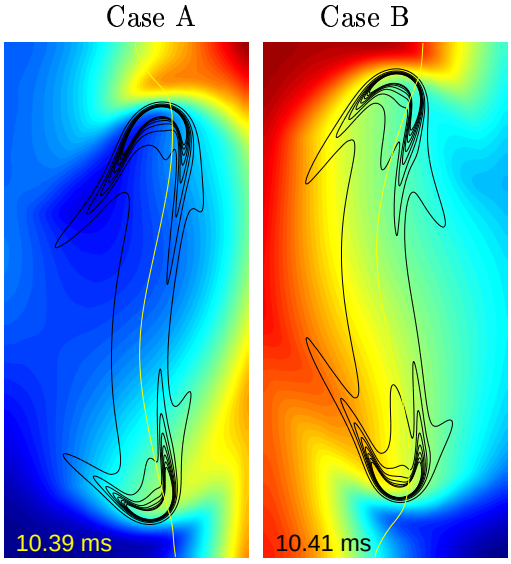

Figure 5: Vertical velocity fields for case A (left), and case B (right). The structure and position of the flame is represented with heat release contours in black and a yellow stoichiometric mixture fraction line.

Internal Edge Flame Structure

We will now focus on the chemical structure of the edge flames at the base of the lifted non-premixed methane-air jet flame. Comparisons of shape and structure of the mole fractions and production rates between the two cases does not reveal significant differences, hence we will focus our discussion on one case, namely case A and the lower edge flame. The structure of the upper flame is very similar. We present results for time $t = 19.1$ ms after applying the heat pulse, when ignition transients have largely vanished.

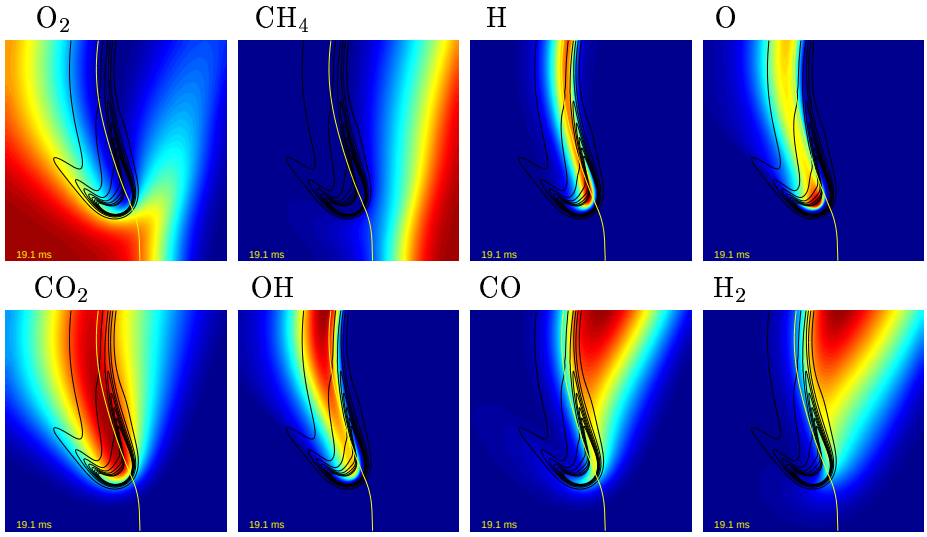

Figure 6: The mole fraction of O_2, CH_4, H and O (top row) and CO_2, OH, CO, H_2 (bottom row) are presented in color. The structure and position of the flame is represented with heat release contours in black, and a yellow stoichiometric mixture fraction line. Domain height is ∼1cm.

Examination of the mole fraction fields of various species in the edge flame region brings up several points of interest. We observe significantly more penetration of O_2 around the edge flame and into the fuel (CH_4) stream than the converse, as seen in Fig. 6. Similar penetration by the oxidizer stream is observed in methanol [6] and hydrogen [18] triple flames. Note that this observation is consistent with the above reported smaller extent of the rich branch, as the concentration of CH_4 rises very quickly on the rich side of the edge flame, such that a higher equivalence ratio is reached faster than on the lean side, despite the more extensive penetration of O_2 into the fuel stream. As can be seen in Fig. 6, H, O, and CO_2 have localized peaks in the edge flame tip region, whereas OH peaks far downstream in the diffusion flame region. We observe a predominance of CO and H_2 on the rich side of the flame. Analysis of the structure of the diffusion flame a short distance (0.6 cm) behind the edge flame tip indicates that CH_4 and O_2 are available on the fuel and air sides respectively, with some O_2 premixing on the fuel-side of the flame. CH_4 and O_2 diffuse and react together in the diffusion flame.

We find that H_2O_2 and HO_2 radicals are predominant at the leading edge of the lean premixed edge-flame branch (Fig. 7). On the other hand, C, CH, CH_2 and CH_2^* concentrations are all aligned in a narrow strip on the fuel-side of the diffusion flame. C_2H_2 - a key soot precursor, is also predominant on the fuel-side of the flame, as might be expected, and peaks far downstream on the fuel-side in diffusion flame region, as can be seen in Fig. 7 in the bottom row. Similarly C_2H_4 and C_2H_6 are on the fuel-side, but extending further into it, with highest C_2H_6 near the rich premixed flame zone, whereas C_2H_4 peaks farther downstream near diffusion flame, more like C_2H_2. As for C_2H_3 and C_2H_5, they exist in narrow strips on the rich side of the edge flame. Their narrow-strip

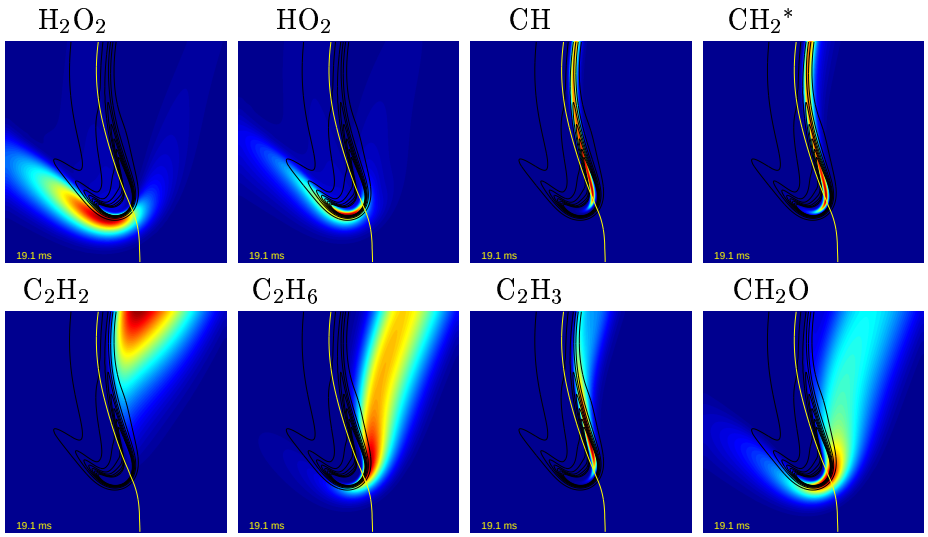

Figure 7: The mole fraction of H_2O_2, HO_2, CH and CH_2* (top row) and C_2H_2, C_2H_6, C_2H_3, and CH_2O (bottom row) are presented in color. The structure and position of the flame is represented with heat release contours in black, and a yellow stoichiometric mixture fraction line. Domain height is ∼1cm.

topology reflects the unstable nature of these radicals, and is consistent with their characteristic structure in a premixed methane-air flame. CH_2O wraps around and peaks in the leading front of the edge flame and extends far into the fuel-side of the flame.

The production rates of all the species shown in Fig. 6 are illustrated in Fig. 8. All these species are consumed or produced predominantly in the premixed flame zone and most of them peak in the lean premixed flame front, except for H_2 and CO that peaks in the rich premixed edge flame branch. O, CO_2, OH and also H_2O production contours are largely confined to the lean side of the premixed front. The consumption of OH and O extends from lean to rich premixed zone and into the diffusion flame zone.

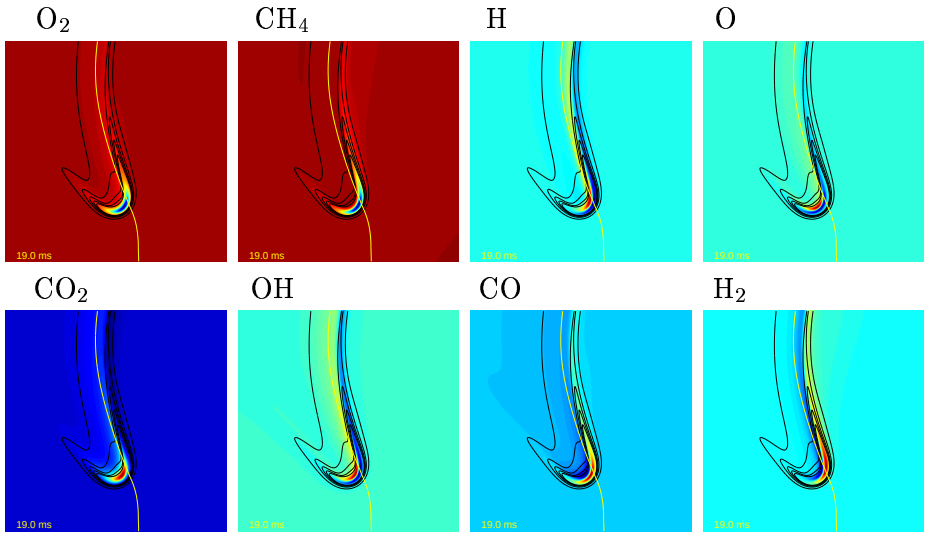

Figure 8: The production rates of O_2, CH_4, H and O (top row) and CO_2, OH, CO, H_2 (bottom row) are presented in color. The structure and position of the flame is represented with heat release contours in black, and a yellow stoichiometric mixture fraction line. Domain height is ∼1cm.

The production rates of the species shown in Fig. 7 are illustrated in Fig. 9. We observe that

H_2O_2 is produced on the leading edge of the edge flame in the cold region and consumed in its immediate downstream vicinity, and it's structure lays mainly on the lean side of the premixed zone. HO_2 structure is similar but does not extend as far in front of the edge flame. CH, CH_2 and CH_2* production rates peak in the premixed zone of the edge flame and extend into the diffusion flame region, aligned in the narrow strip on the rich side of the diffusion flame. C_2H structure is very similar but peaks higher in the diffusion flame zone. C_2H_2, a soot precursor, reveals very different reaction rate structure, much wider and with the peak consumption and production far downstream in the diffusion flame region. Its topology extends more into the rich side of the flame. C_2H_6 and also C_2H_5 production rate profiles extend from lean to rich premixed flame fronts, whereas C_2H_3 production is confined mostly to the rich premixed flame zone. CH_2O is produced on the leading edge of the premixed fronts, both lean and rich side.

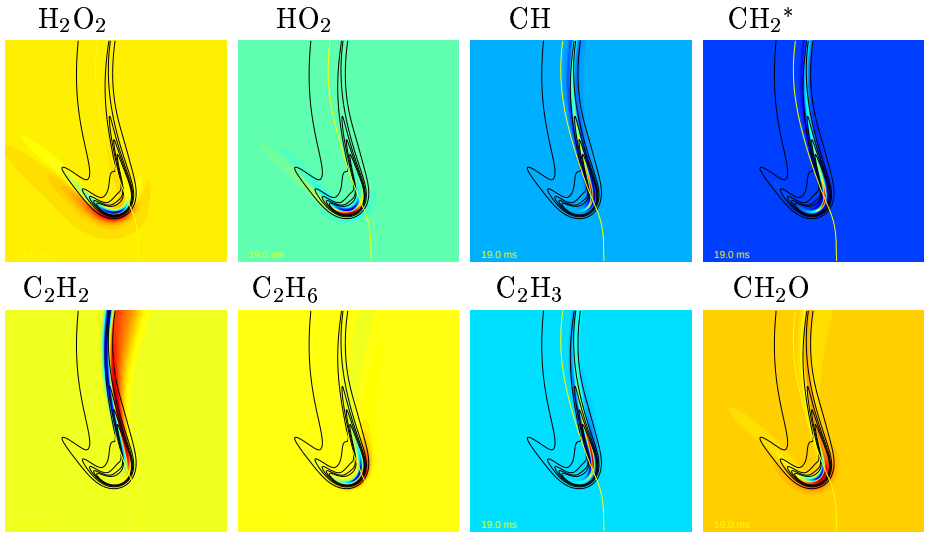

Figure 9: The production rates of H_2O_2, HO_2, CH and CH_2* (top row) and C_2H_2, C_2H_6, C_2H_3, and CH_2O (bottom row) are presented in color. The structure and position of the flame is represented with heat release contours in black, and a yellow stoichiometric mixture fraction line. Domain height is ∼1cm.

Comparison with Experiment

The comparison between computational and experimental (PLIF) CO and OH data is presented in Fig. 10. The experimental setup is described in detail in Rehm and Paul [19]. A circular N_2-diluted methane jet was used, surrounded by annular co-flow air, obtaining a stable lifted non-premixed flame. The measured CO and OH fields are proportional to species concentration fields, but do not directly represent mole fraction, due to the chosen temperature-dependence in the laser-induced fluorescence (LIF) signal magnitude. One can notice that the CO pool curves around the leading edge of the flame towards the lean side and is bordered by OH on the diffusion flame side with some overlap. The comparison of topology and structure of these two species between numerical and experimental data shows very good qualitative agreement. The measurements of CO and OH were performed simultaneously. With proper selection of excitation transition the product of these two signals was shown to provide a spatial marker of the forward reaction OH+CO→H+CO_2 (R99) as well as a measure of the relative forward rate of this reaction. The right column of Fig. 10 shows the experimental product image (top) as well as the computed forward rate of R99 (bottom). Again, the experimental and numerical data show very good qualitative agreement. Further, the left frame

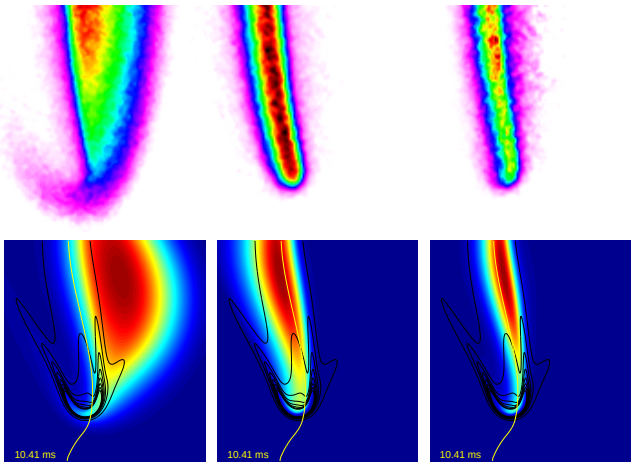

Figure 10: The top row presents experimental (PLIF) data, and the bottom shows corresponding numerical simulation data. The left column shows CO, the middle column shows OH and the right column shows the computed forward reaction rate R99 ($OH + CO \rightarrow H + CO_2$) (bottom) and the experimental OH-CO PLIF signal product (top). Numerical data: blue is mapped to the lowest value, red to the highest; heat release rate is shown as contours, the yellow line is the stoichiometric mixture fraction line. The lower flame in case B is presented; frame height is 1cm. Experimental data: magenta is mapped to the lowest value, red to black to the highest; frame height is 1cm.

in Fig. 11 presents the computed concentration product [CO][OH], showing an excellent correlation with the computed forward rate of R99, shown in Fig. 10. The reverse reaction rate field of R99 is topologically similar to the forward rate, leading to cancellation in the hot region and a net reaction rate structure that correlates well with heat release topology and is confined to the premixed region (Fig. 11 middle frame). The production rate of CO_2 is shown in the right frame in Fig. 11, and correlates very well with the net rate of R99, exhibits the same topology as the net reaction rate of R99, which is consistent with the dominance of this reaction in CO_2 production.

The CO measurements were corrected for optical interference from photochemically produced C_2^*. Seitzmann *et al.* [20] suggested that the photofragmentation of C_2H_2 was the most likely source of C_2^* in non-sooting flames. Based in part on the results of Fahr *et al.* [21], Rehm and Paul [19] suggested that an alternate source of C_2^* is the photofragmentation of C_2H_3. A comparison of the topology of the experimental results and the numerical C_2H_2 and C_2H_3 concetration fields suggest that both C_2H_2 and C_2H_3 contribute to the C_2^* signal, and that the C_2^* signal is likely about 100 times more sensitive to C_2H_3 than to C_2H_2.

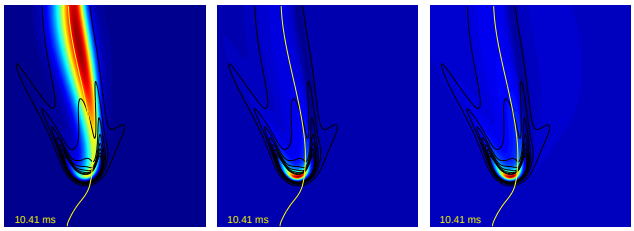

Figure 11: The concentration product [CO][OH] is shown in the left frame, the net rate of progress of reaction R99 is in the middle and the production rate of CO_2 is presented in the right frame. Heat release rate is shown as contours. The yellow line is the stoichiometric mixture fraction line. The lower flame in case B is presented; the frame height is 1cm.

Finally, it has been shown that HCO is a good choice of observable for heat release measurements [22, 23] in premixed methane-air flames. Paul and Najm [24] also showed that the product of CH_2O and OH PLIF signals can be made proportional to the forward bimolecular rate, that correlates well with heat release rate. We find that these observations are also true in the computed

edge flame. In Fig. 12 we present the structure of the mole fraction field of CH_2O and OH and their concentration product. CH_2O is concentrated in the premixed zone on the leading edge of the flame and extends far into the rich premixed flame zone. OH is largely confined to the diffusion flame zone. The product of CH_2O and OH concentrations exhibits very different topology and is limited to the region of high heat release, and hence is a good marker for heat release rate and topology in the edge flame. The forward reaction rate of reaction R101: $OH + CH_2O \rightarrow HCO + H_2O$, is also presented in Fig. 12 along with the heat release rate and the mole fraction of HCO (bottom row) and show very good correlation of all three along with the concentration product of CH_2O and OH. This confirms that HCO as well as concentration product of CH_2O and OH (easier to measure experimentally) are good experimental observables for heat release rate and edge flame topology in methane-air edge flames.

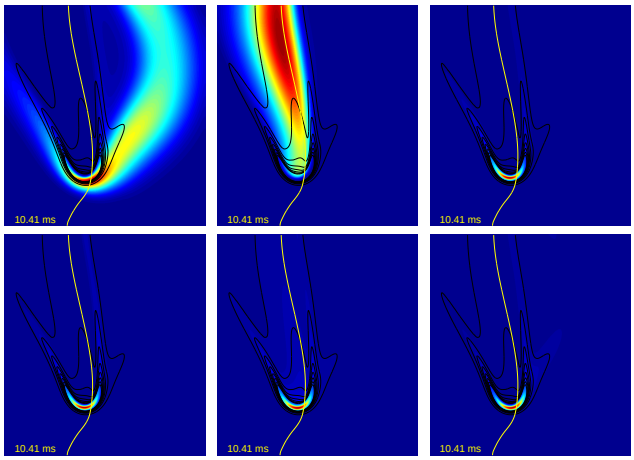

Figure 12: Top row, left to right: Mole fraction of CH_2O is shown in the left frame and mole fraction of OH in the middle frame, and concentration product of $[CH_2O][OH]$ in the right frame. Bottom row: forward rate of reaction R101 ($OH + CH_2O \rightarrow HCO + H_2O$), the heat release rate and HCO mole fraction is presented. Blue is mapped to the lowest value, red to the highest; the heat release rate is shown as contours. The yellow line is the stoichiometric mixture fraction line. The lower flame in case B is presented; the frame height is 1cm.

Conclusions

Edge flame structure and topology in a 2D laminar methane-air jet was studied numerically and experimentally. Ignition in the computed jet mixing layer was achieved by localized heating, creating a circular premixed flame front that rapidly grows and moves towards the stoichiometric mixture fraction line, penetrates it, and propagates along it, forming two edge flame structures that move up and down the line. Two different cases were studied, case A with faster jet fluid and case B with faster coflow. The motivation for studying these two configurations was to investigate the effect of the velocity field on the structure and development of edge flames, thereby discriminating between shear layer and mixing layer roles in defining edge flame structure. Despite the flow-field differences, the developed edge flames do not show significant difference in internal structure. The heat release contours initially span lean and rich premixed flame branches, but eventually the rich branch of heat release rate contours aligns along the rich side of the diffusion flame edge, and becomes very small. This is shown to be due to uneven equivalence ratio variation on the lean and the rich sides immediately in front of the leading edge of the flame. The high equivalence ratio gradient on the rich side causes the premixed wing to quickly subside with distance from the stoichiometric mixture fraction line. The maximum heat release rate is located on the lean side in both cases, as was also

observed in a hydrogen-air triple flame [7]. The shear layer affects the edge flame orientation and the stretching of the lean and rich premixed branches, while the mixing layer defines edge flame internal structure, topology and position relative to the stoichiometric mixture fraction line. The edge flames exist on the oxidizer side, and not in the slower fluid region. The edge flame structure was described and compared to experimental data from PLIF measurements of OH and CO, as well as forward reaction rate. Excellent qualitative agreement was demonstrated. We showed that the concentration product of OH and CO is a good marker for the forward rate of the reaction $CO+OH=CO_2+H$ in the edge flame, and that the production rate of CO_2 is well correlated with heat release rate. The concentration product of CH_2O and OH, as well as the mole fraction of HCO are also shown to be a good experimental observables for heat release rate and topology of edge flames

Acknowledgements

This work was supported by the US Dept. of Energy, Office of Science, Office of Basic Energy Science, Division of Chemical Sciences, Geosciences, and Biosciences.

References

[1] Muñiz, L., and Mungal, M.G., *Combustion and Flame*, 111:16–31 (1997).

[2] Lee, B.J., and Chung, S.H., *Combust. Flame*, 109:167 (1997).

[3] Ghosal, S., and Vervisch, L., *Combust. Flame*, 123:646 (2001).

[4] Reutsch, G.R., Vervisch, L., and Linan, A., *Phys. Fluids*, 7:1447 (1995).

[5] Daou, J., and Linan, A., *Combust. Theory Modelling*, 2:449 (1998).

[6] Echekki, Tarek, and Chen, Jacqueline, *Combustion and Flame*, 114:231–245 (1998).

[7] Im, H.G., and Chen, J.H., *Combust. Flame*, 126:1384 (2001).

[8] Mueller, C.J., and Schefer, R.W., *Proc. Comb. Inst.*, 27:1105–1112 (1998).

[9] Kioni, P.N., Bray, N.C., Greenhalgh, D.A., and Rogg, B., *Combust. Flame*, 116:192 (1999).

[10] Plessing, T., Terhoeven, P., Peters, N., and Mansour, M.S., *Combust. Flame*, 115:335 (1998).

[11] Najm, H.N., Schefer, R.W., Milne, R.B., Mueller, C.J., Devine, K.D., and Kempka, S.N., Technical Report SAND98-8232, Sandia National Labs., Alb., New Mexico, (1998).

[12] Devine, K., and Flaherty, J., *Appl. Numer. Math.*, 20:367–386 (1996).

[13] Ray, J., Najm, H.N., Milne, R.B., Devine, K.D., and Kempka, S.N., *Proc. Comb. Inst.*, 28:219–226 (2000).

[14] Najm, H.N., Milne, R.B., Devine, K.D., and Kempka, S.N., *ESAIM Proceedings*, volume 7, pp. 304–313, (1999).

[15] Frenklach, M., Wang, H., Goldenberg, M., Smith, G.P., Golden, D.M., Bowman, C.T., Hanson, R.K., Gardiner, W.C., and Lissianski, V., Top. Rep. GRI-95/0058, GRI, (1995).

[16] Brown, P.N., Byrne, G.D., and Hindmarsh, A.C., *SIAM J. Sci. Stat. Comput.*, 10:1038–1051 (1989).

[17] Bilger, R.W., Starner, S.H., and Kee, R.J., *Comb. and Flame*, 80:135–149 (1990).

[18] Im, H.G., and Chen, J.H., *Combust. Flame*, 119:436 (1999).

[19] Rehm, J., and Paul, P.H., *Proc. Comb. Inst.*, 28:1775–1782 (2000).

[20] Seitzman, J.M., Haumann, J., and Hanson, R.K., *Applied Optics*, 26:2892–2899 (1987).

[21] Fahr, A., Hassanzadeh, P., and Atkinson, D.B., *Chem. Phys.*, 236:43 (1998).

[22] Najm, H.N., Paul, P.H., Mueller, C.J., and Wyckoff, P.S., *Combustion and Flame*, 113(3):312–332 (1998).

[23] Najm, H.N., Knio, O.M., Paul, P.H., and Wyckoff, P.S., *Comb. Sci. Tech.*, 140(1-6):369–403 (1998).

[24] Paul, P.H., and H.N.Najm *Proc. Comb. Inst.*, 27:43–50 (1998).